A resilient adaptive sliding mode observer for sensorless AC salient pole machine drives based on an improved HF injection method

Amir Messali, Malek Ghanes, Mohamed Assaad Hamida, M. Koteich

A resilient adaptive sliding mode observer for sensorless AC salient pole machine drives based on an improved HF injection method

A. Messali[1], M. Ghanes [1,*], M A. Hamida [1] and M. Koteich [2]
[1] Ecole Centrale de Nantes, LS2N UMR CNRS 6004, Nantes, France.
[2] Renault Group, Technocentre, Guyancourt, France.
[*] Corresponding author: malek.ghanes@ec-nantes.fr

Abstract

In high frequency (HF) injection methods, classical tracking algorithms are used to estimate the rotor position for sensorless alternating current (AC) salient pole machines. These algorithms were dependent on AC machine inductances which are characterized by their large variations. To overcome this dependency, a new approach based on using only the sign of the rotor position estimation error (instead of using rotor position estimation error) is proposed. This approach has also the advantage of removing the low-pass filter (LPF) used to separate the HF component from the rotor position information. Consequently, only the first order sliding mode observer can be employed to estimate the rotor position, as only the sign of the rotor position estimation error is known. To avoid the well known chattering phenomena of this observer, an adaptive step-by-step sliding mode observer is proposed as an alternative solution to estimate the rotor position of the machine. The stability study of the proposed observer is analyzed both in transient/steady state ranges and a procedure for gains tuning is then given. The performance of the proposed algorithm is tested on simulation and experimentally in the framework of a representative small-scale electric propulsion benchmark, used in automotive applications. Moreover, a comparison study is conducted with respect to some existing tracking algorithms in order to illustrate the well-founded of the designed algorithm.

Keywords: First order sliding mode observers, adaptive gains, step-by-step observer, sensorless control, HF signal injection, AC salient pole machines, experimental results, comparison study.

Nomenclature

IPMSM	Interior Permanent Magnet Synchronous Motor
PLL	Phase-Locked-Loop
MSO	Mechanical System Observer
$\underline{x}$	Complex notation of x
$\underline{x^*}$	Conjugated component of x
R_s	Stator resistance
L_d, L_q	dq-axis inductances
L_0, L_2	Average and differential inductances, respectively
ψ_m	Permanent-magnet flux linkage
$\underline{\psi_s^s}$	Stator flux linkage vector presented in the stator reference frame
$\underline{v_s^s}$	Stator voltage vector presented in the stator reference frame
$\underline{i_s^s}$	Stator current vector presented in the stator reference frame
$\underline{i_s^{r*}}$	Conjugated stator current vector presented in the rotating reference frame
$\underline{\psi_s^r}$	Stator flux linkage vector presented in the rotating reference frame
ψ_d, ψ_q	dq stator flux linkage presented in the rotating reference frame
i_d, i_q	Stator currents presented in the rotating reference frame
$\underline{v_{sc}^{\hat{r}}}$	HF injected voltage vector presented in the estimated reference frame
V_c, ω_c	Amplitude and frequency of the HF injected voltage
$\underline{v_{sc}^s}$	HF injected voltage vector presented in the stator reference frame
$\underline{\psi_{sc}^s}$	HF flux linkage vector presented in the stator reference frame
$\underline{\psi_{sc}^{s*}}$	Conjugated HF flux linkage vector presented in the stator reference frame
$\underline{i_{sc}^s}$	HF Stator current vector presented in the stator reference frame
$\underline{i_{s1}^s}$	Fundamental current component
e_θ	Rotor position estimation error
I_{cp}	Magnitude of HF positive current component
I_{cn}	Magnitude of HF negative current component
ω	Electrical rotor speed
θ	Electrical rotor position
ϵ	Rotor position estimation error
J	Moment of inertia
K_f	Viscous friction coefficient
p	Number of pole pairs
T_l	Load torque
T_m	Electromagnetic torque.

1. Introduction

1.1. Problem statement

AC machines drive requires expensive and cumbersome position sensors [1]. To deal with these limitations, two principle techniques called model based and saliency based methods

were proposed in the literature. The model-based methods [2], [3], [4], [5] use the mathematical model to enable access to the rotor and speed estimation of AC salient pole machines. The demerits of this method are principally the non-modeled dynamics, the observability at low and zero speeds and the parameter uncertainties [6], [7].
The saliency-based method [8], [9], [6] was proposed as alternative to deal with limitations of the model-based methods [8]. But in reality these methods are still dependent on some machine parameters since the rotor position estimation error is function of machine inductances which can vary significantly according to various causes [8], [10], [11]. The tracking algorithms used in the literature (PLLs [12] [13], MSO [14]) to estimate the rotor position and speed based on the extracted rotor position estimation error are sensitive to machine parameter variations and to acceleration effects (transient modes).

1.2. Contribution

In this paper the contribution is twofold. First, an innovative methodology that uses only the sign of the rotor position estimation error as shown in Figure 1. The aim of Part1 is to get rid of machine inductances and to remove the LPF usually used in the pulsating HF signal injection method to reduce the cost and complexity of implementation. The idea of getting rid of machine inductances has been introduced in [6] and it was associated with the square-wave (not pulsating) HF signal injection method. However, the square-wave ([15], [16]) HF signal injection method generates non negligible acoustic noise, requires sensitive current sensors and generates harmonics on the rotor position and speed estimation [17]. The improved pulsating HF signal injection method proposed in this paper, doesn't require sensitive current sensors. Moreover, the generated harmonics on the rotor position and speed estimation are significantly reduced by the proposed method as well as the acoustic noise.
By having only the sign of the rotor position estimation error as a known information, the first order sliding mode observer is the natural solution to estimate the rotor position, as it was proposed in [6] with constant gains. However, in this case, it is well known that this type of observers suffer from chattering phenomena [18, 19, 20, 21, 22, 23, 24, 25, 26, 27, 28, 29, 30, 31]. This phenomena can be reduced by using a low pass filter, but this solution generates delays and increases the cost and the complexity of the implementation. That is why, the second contribution (part 2 of figure 1) of this paper is dedicated to propose a new step-by-step sliding mode observer with adaptive gains, in order to estimate the rotor position and speed with less chattering and with an easy tuning of the observer. Moreover, the acceleration is estimated to improve the position estimation in transient modes and a complete stability analysis is given to ensure the observer convergence in steady-state, transient and intermediate modes. It is worth noticing that in [6], the sliding mode observer with constant gains is not proposed with a step-by-step procedure of estimation. Consequently the tuning of this observer is not done in a decoupled manner that makes this tuning not easy. Moreover, the stability analysis of this observer is a classical one.
To point out the contributions in simulation and experiments, the performances of the proposed adaptive gains step-by-step observer based on an improved pulsating HF signal injection method are compared with the classical tracking algorithms and step-by-step sliding mode observer with constant gains. Both algorithms are associated with the same HF signal

injection method as for the step-by-step observer with adaptive gains, i.e., the improved pulsating HF signal injection method.
The HF injection process can be divided into two parts (Parts 1 and 2), as illustrated in figure 1.

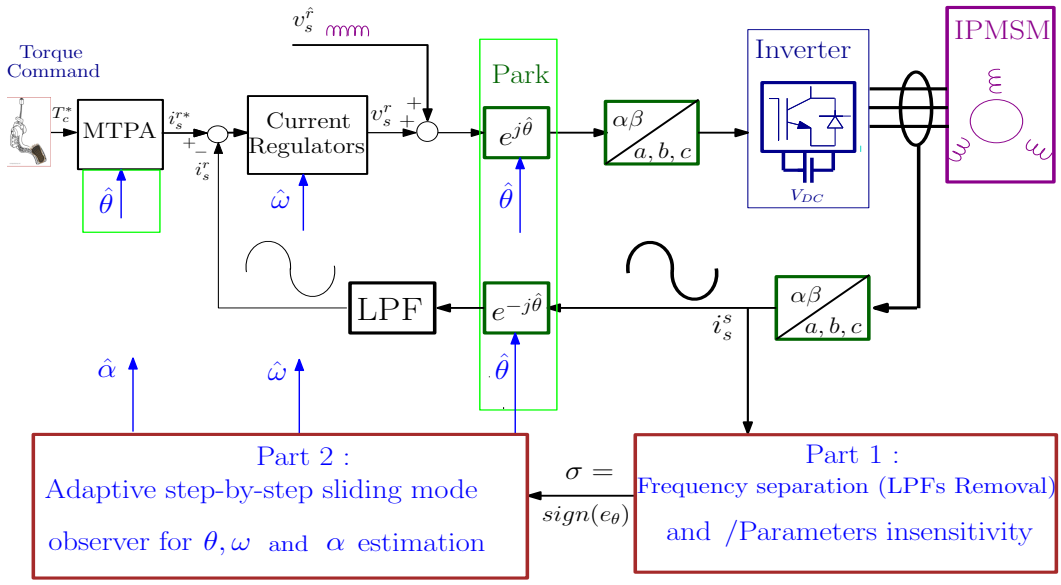

Figure 1: Self-sensing control of AC salient pole machines.

As it can be seen in Figure 1, the estimation process (Part 1 and Part 2) don't depend on the controller design. They depend only on the injected high frequency voltage.

1.3. Paper organization

The rest of the paper is organized as follows. Section 2 recalls the existing tracking algorithms. The IPMSM modeling is introduced in Section 3. The pulsating HF voltage injection technique is presented in Section 4. In section 5, parts 1 and 2 (Figure 1) of position/speed estimation strategy are introduced in details. Simulation and experimental results are presented in Section 6, where an electrical propulsion profile in automotive applications is used. A comparative study with existing techniques is given in the same section. Conclusions and perspectives are given in section 7.

2. Existing Tracking Algorithms

PLLs [32] and MSO [33] are tracking observers mainly used in the literature to estimate the rotor position and speed based on the extracted rotor position estimation error using HF signal injection methods. These tracking algorithms will be briefly recalled in this section in order to compare their performances with the proposed algorithm introduced in section 5.2. Moreover, the step-by-step sliding mode observer with constant gains is given to compare its performances with the proposed algorithm.

2.1. Phase Locked Loop

The PLL is one of the observer algorithm mostly used in the literature for the speed and position estimation. The PLL algorithm is showed in Figure (5) and given by

$$\dot{\hat{\omega}} = K_{\omega,p}\ \epsilon \tag{1}$$

$$\dot{\hat{\theta}} = \hat{\omega} + K_{\theta,p}\ \epsilon \tag{2}$$

where the ε is the rotor position estimation error. Gains $K_{\omega,p}$ and $K_{\theta,p}$ are chosen according to the stability analysis given by [32].

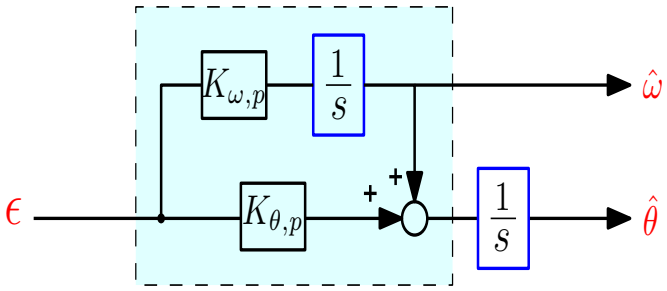

Figure 2: Block-diagram of PLL estimator.

2.2. Mechanical system observer

Mechanical system observer (MSO) [33] is used to estimate the rotor position and speed. The estimation is based on the rotor position error. As mentioned in the previous section, the rotor position error depends on the machine inductances which affect the estimation, furthermore MSO requires the accurate knowledge of the mechanical parameters which is not the case in practice. The dynamic equation of the mechanical system is expressed as follows

$$J\ p\ \dot{\omega} + K_f\ p\ \omega = T_m - T_l$$

The mechanical system observer enhanced by steady-state load torque estimation is shown in Figure 3 and expressed by following system equations

$$\dot{\hat{\theta}} = \hat{\omega} + K_{\theta,s}\ \epsilon \tag{3}$$

$$\dot{\hat{\omega}} = \frac{1}{J}[T_m - \hat{T}_l - K_f\hat{\omega}] + K_{\omega,s}\ \epsilon \tag{4}$$

$$\dot{\hat{T}}_l = K_{T,s}\ \epsilon \tag{5}$$

where $K_{\theta,s}$, $K_{\omega,s}$ and $K_{T,s}$ are the observer gains.

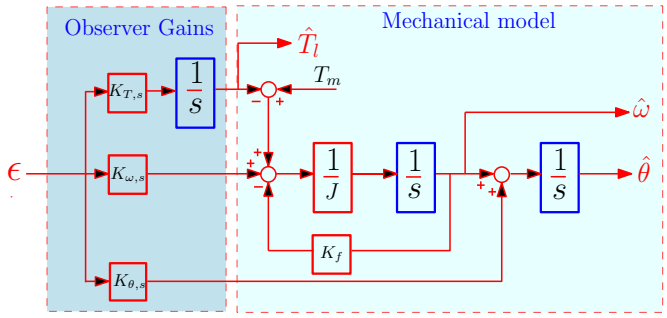

Figure 3: Block-diagram of MSO.

The PLL and MSO widely used in the literature for sensorless control of AC machines are recalled in this section in order to compare their performances with respect to proposed method in the sequel.

3. IPMSM Modeling

In this section, voltage and flux-current IPMSM models are presented. The first part introduces the classical model [34] without HF injection. The second part is mainly reserved for HF models [35].

3.1. Classical model of IPMSM

The voltage-flux model in the stator reference frame and the flux-current model in the rotor frame are described by equations (6) and (7) as follows

$$\underline{v_s^s} = R_s \underline{i_s^s} + \frac{d\underline{\psi_s^s}}{dt} \tag{6}$$

$$\underline{\psi_s^r} = \psi_d + j\psi_q \tag{7}$$

where,

$$\psi_d = L_d i_d + \psi_m, \quad \psi_q = L_q i_q \tag{8}$$

By replacing (8) in (7), the following expression is obtained

$$\underline{\psi_s^r} = L_0 \underline{i_s^r} + L_2 \underline{i_s^{r*}} + \psi_m \tag{9}$$

where, $L_0 = \frac{L_d+L_q}{2}$ and $L_2 = \frac{L_d-L_q}{2}$.
The stator magnetic flux vector can be expressed in the stator reference frame by using Park transformation for equation (9) as follows

$$\underline{\psi_s^s} = L_0 \underline{i_s}^s + L_2 \underline{i_s}^{s*} e^{j2\theta} + \psi_m e^{j\theta}. \tag{10}$$

3.2. High Frequency IPMSM models

The following assumptions are regarded to build the HF IPMSM models.

- The stator resistance R_s is overlooked in front of the self-stator reactance $j\omega_c L_s$ ($(R_s << j\omega_c L_s)$).
- The cross saturation effect and the rotating back-EMF are neglected.

Considering above assumptions, HF voltage-flux and flux-current relationships [35] in stationary frame are given by following equations

$$\underline{v_{sc}^s} \simeq \frac{d\underline{\psi_{sc}^s}}{dt}. \tag{11}$$

$$\underline{\psi_{sc}^s} = L_0 \underline{i_{sc}^s}^{\,s} + L_2 \underline{i_{sc}^{s*}} e^{j2\theta}. \tag{12}$$

From (12), the current expression is deduced

$$\underline{i_{sc}^s} = \frac{1}{{L_0}^2 - {L_2}^2}(L_0 \underline{\psi_{sc}^s} - L_2 \underline{\psi_{sc}^{s*}} e^{j2\theta}). \tag{13}$$

For clear understanding the operation of the proposed sensorless control method, the pulsating [36], [37] voltage injection technique adopted in this paper is introduced in next section.

4. Pulsating injection-based method

4.1. HF Injected signal form

The pulsating technique exploited in this paper [9] consists of injecting a HF voltage into the estimated $\hat{d}$ axis as illustrated in Figure 4, which can be expressed as

$$\underline{v_{sc}^{\hat{r}}} = -V_c \sin(\omega_c t) \begin{bmatrix} 1 \\ 0 \end{bmatrix} \tag{14}$$

The injected pulsating voltage vector in the estimated reference frame is shown by Figure 4.

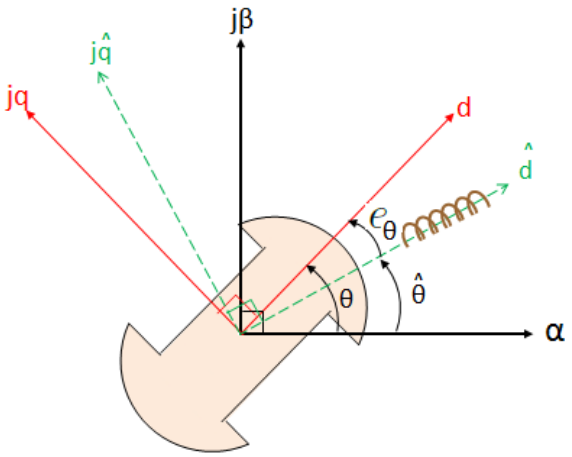

Figure 4: HF voltage injection pulsating principle.

By using Park transform, the expression of the HF injected voltage in the stator reference frame is given by

$$\underline{v_{sc}^{s}} = -V_c \sin(\omega_c t) e^{j\hat{\theta}}. \tag{15}$$

4.2. HF Flux-Current generated by the injected signal

By integrating the injected stator voltage given in (15), the following HF stator flux expression is obtained

$$\underline{\psi_{sc}^{s}} = \int -V_c \sin(\omega_c t) e^{j\hat{\theta}} dt = \frac{V_c}{\omega_c} \cos(\omega_c t) e^{j\hat{\theta}}. \tag{16}$$

The HF stator current expression can be obtained by combining (16) and (13)

$$\underline{i_{sc}^{s}} = \frac{V_c}{\omega_c({L_0}^2 - {L_2}^2)} (L_0 e^{j\hat{\theta}} - L_2 e^{j(2\theta - \hat{\theta})}) \cos(\omega_c t) \tag{17}$$

By taking the fundamental current component i_{s1}^{s} into account, the general stator current can be expressed as

$$\underline{i_{s}^{s}} = I_{cp} \cos(\omega_c t) e^{j\hat{\theta}} - I_{cn} \cos(\omega_c t) e^{j(2\theta - \hat{\theta})} + i_{s1}^{s} \tag{18}$$

where

$$e_\theta = \theta - \hat{\theta}, \tag{19}$$

$$I_{cp} = \frac{L_0 V_c}{\omega_c(L_0^2 - L_2^2)}, \tag{20}$$

$$I_{cn} = \frac{L_2 V_c}{\omega_c(L_0^2 - L_2^2)} = \frac{(L_d - L_q)V_c}{\omega_c L_d L_q}, \tag{21}$$

5. Proposed Position Estimation Strategy

In this section, two parts are introduced. The first part allows to parameters insensitivity and LPF removal that improve the accuracy and robustness of the rotor position and speed estimation strategy. The second part focuses on a new adaptive step-by-step sliding mode tracking algorithm for self-sensing control of AC salient pole machines without knowing machine parameters (inductances, viscous coefficient, inertia) and HF signal characteristics. The machine acceleration is estimated to compensate the rotor position and speed estimation errors in transient modes and to improve performances compared to traditional techniques. The resulting HF current expression of AC salient pole machines in the estimated reference frame $i_s^{\hat{r}}$ frame (see Figure 4), without the fundamental component[1] is given by

$$i_s^{\hat{r}} = \begin{bmatrix} i_{\hat{d}c} \\ i_{\hat{q}c} \end{bmatrix} = \begin{bmatrix} I_{cp} - I_{cn} \cos 2(e_\theta) \\ -I_{cn} \sin 2(e_\theta) \end{bmatrix} \cos(\omega_c t) \tag{22}$$

[1]The fundamental frequency is removed by using a high pass filter (HPF)

The rotor position estimation error expression (19) can be deduced from the second component of (22), $i_{\hat{q}c}$, which depends only on I_{cn} (21)

$$\rho \quad = \quad i_{\hat{q}c} = -I_{cn} \sin[2(e_\theta)] \cos(\omega_c t). \tag{23}$$

Then, (23) is multiplied by $\cos(\omega_c t)$

$$\epsilon = \rho * \cos(\omega_c t) = -I_{cn} \sin[2(e_\theta)][\cos(\omega_c t)]^2. \tag{24}$$

5.1. Part 1: parameters insensitivity and LPFs removal

This first part allows:

- to extract the rotor position information by using the sign of the rotor position estimation error in order to get rid the machine inductances,
- to remove the LPF used in HF injection method in order to separate the high frequency (ω_c) component from the low frequency ($2(e_\theta)$).

In the literature, the term $[\cos(\omega_c t)]^2$ is always removed by using LPFs, and I_{cn} in (21), which is function of machine inductances and HF injected signal characteristics, is often considered as a constant gain, which is a strong assumption.

In this paper, an approach to remove LPFs and to avoid inductances knowledge requirement is proposed.

It is known that $[\cos(\omega_c t)]^2 \geqslant 0$. Moreover, for all AC salient pole machines the condition of $-I_{cn} > 0$ is always satisfied because $L_q > L_d$. One has also $V_c > 0$ and $\omega_c > 0$. Consequently by applying the sign function to (24), the expression of the rotor position estimation error becomes independent of I_{cn} in (21) (machine inductances and injection signal characteristics) as follows

$$\sigma = sign(\epsilon) = sign(\sin(2e_\theta)). \tag{25}$$

For all $e_\theta \in [-\frac{\pi}{2}; \frac{\pi}{2}]$, σ in (25) becomes

$$\sigma = sign(e_\theta) \tag{26}$$

where $sign(e_\theta)$ is sign function defined as in [38]:

$$sign(e_\theta) : \begin{cases} 1 \quad \text{if} \quad e_\theta > 0 \\ -1 \quad \text{if} \quad e_\theta < 0 \\ \in [-1 + 1] \quad \text{if} \quad e_\theta = 0. \end{cases} \tag{27}$$

From (26), it is confirmed that the HF component can be removed without using LPFs and it can be seen that the new rotor postion estimation error σ is no longer dependent on machine parameters (L_d, L_q) and injected signal characteristics (V_c, ω_c).

The proposed technique is valid as long as the position error belongs to $e_\theta \in [-\frac{\pi}{2}; \frac{\pi}{2}]$. This includes situations when the motor suddenly gets blocked, or slows down due to some unpredictable circumstances, or when the initial rotor position is wrong.

The sign of the estimation error σ in (26) is used instead of ϵ in (24) as a known information in a new step-by-step tracking algorithm, which has a finite time convergence. This algorithm, which is the subject of Part 2, aims to estimate the rotor position, speed and acceleration of AC salient pole machines without knowing machine parameters and with less chattering.

5.2. *Part 2: Adaptive Step-by-step sliding mode observer for rotor position, speed and acceleration estimation*

The rotor position estimation error σ (26), extracted in Part 1, will be used by the second part to estimate the position, speed and the acceleration of AC salient pole machines without knowing machine parameters (inductances, viscous coefficient, inertia) and HF signal characteristics. Note that the machine acceleration will be also estimated to compensate the rotor position and speed estimation errors in transient modes and to improve performances compared to traditional techniques. To make the tuning procedure of rotor position, speed and acceleration estimation technique easier, a robust adaptive step-by-step observer is proposed that ensures the finite time convergence of the rotor position, speed and acceleration states and reduces the chattering effect on the rotor and speed estimations.

5.2.1. *Observer design*

Based on the sign of rotor position estimation error (26), adaptive step-by-step sliding mode observer (28)–(32) is proposed to estimate the rotor position, speed and acceleration of AC salient pole machines

$$\dot{\hat{\theta}} = \hat{\omega} + [K_{\theta_{max}} - E_1 \ f_1] sign(e_\theta) \tag{28}$$

$$f_1 = K_{\theta_{max}} - K_{\theta_{min}} - (K_{\theta_{min1}} - K_{\theta_{min}}) \frac{|\hat{\omega}|}{\omega_{max}} \tag{29}$$

$$\dot{\hat{\omega}} = \hat{\alpha} + E_1 [K_{\omega_{max}} - E_2 \ f_2] sign(\bar{\omega} - \hat{\omega}) \tag{30}$$

$$f_2 = K_{\omega_{max}} - K_{\omega_{min}} - (K_{\omega_{min1}} - K_{\omega_{min}}) \frac{|\hat{\alpha}|}{\alpha_{max}} \tag{31}$$

$$\dot{\hat{\alpha}} = E_2 K_\alpha sign(\bar{\alpha} - \hat{\alpha}) \tag{32}$$

where,

$$\bar{\omega} = \hat{\omega} + K_{\theta_{max}} sign(e_\theta) \tag{33}$$

$$\bar{\alpha} = \hat{\alpha} + K_\alpha sign(\bar{\omega} - \hat{\omega}) \tag{34}$$

$$E_1 : \begin{cases} 1 & \text{if} \quad g(k) = 0 \\ 0 & \text{if} \quad \text{whereas,} \end{cases} \tag{35}$$

$$E_2 : \begin{cases} 1 & \text{if} \quad E_1 = 1 \quad \text{and} \quad \bar{\omega} - \hat{\omega} = 0 \\ 0 & \text{if} \quad \text{whereas,} \end{cases} \tag{36}$$

and

$$g(k) : \begin{cases} = 0 & if \quad |\sigma(k) + \sigma(k-1)| + |\sigma(k-1) + \sigma(k-2)| = 0 \\ \neq 0 & else \end{cases} \tag{37}$$

with $\sigma[k]$ is the discrete form of the temporal function $\sigma[t]$, k is the delay of one time step by one control period in the discrete domain.

Remark 1. *The function $g(k)$ is introduced to detect the chattering phenomenon, because as mentioned before only the sign of the position error is available as a known information for the observer. More precisely, at the beginning the observer is supposed to be in transient, then $E_1 = 0$, in this case maximum observer gains are applied. When the value of σ changes twice during three sampling times, then $g(k) = 0$ which gives $E_1 = 1$ the observer is in steady state. In this case the applied gains are less than the maximum ones in order to reduce the chattering. The passage from steady state to transient can be detected when σ doesn't change value after one sampling time, then $g(k) \neq 0$ which gives $E_1 = 0$. In this case maximum observer gains are applied.*

The proposed virtual system for the observer design (28)–(32) is given by

$$\dot{\theta} = \omega \tag{38}$$

$$\dot{\omega} = \alpha \tag{39}$$

$$\dot{\alpha} = 0 \tag{40}$$

In the literature, the rotor speed is usually considered constant which affects the estimation performances in transient modes. Mechanical parameters should be well known when dynamics of speed are taken into account, especially for drive application. The proposed virtual system (38)–(40) makes it possible to overcome limitations of accurate knowledge of mechanical parameters. In addition, the constant speed assumption is not needed if the acceleration of the machine is taken into account in the estimation process. All these assets allow to improve the rotor position and speed estimation both in transient and steady-state modes.

5.2.2. Stability analysis based on the sign propagation

Consider (19), (41) and (42) the position, the speed and the acceleration estimation errors between observer (28)–(32) and system (38)–(40)

$$e_\omega = \omega - \hat{\omega} \tag{41}$$

$$e_\alpha = \alpha - \hat{\alpha} \tag{42}$$

whose dynamics are given by

$$\dot{e}_\theta = e_\omega - [K_{\theta_{max}} - E_1 \ f_1] sign(e_\theta) \tag{43}$$

$$\dot{e}_\omega = e_\alpha - E_1 [K_{\omega_{max}} - E_2 \ f_2] sign(\bar{\omega} - \hat{\omega}) \tag{44}$$

$$\dot{e}_\alpha = -E_2 K_\alpha sign(\bar{\alpha} - \hat{\alpha}) \tag{45}$$

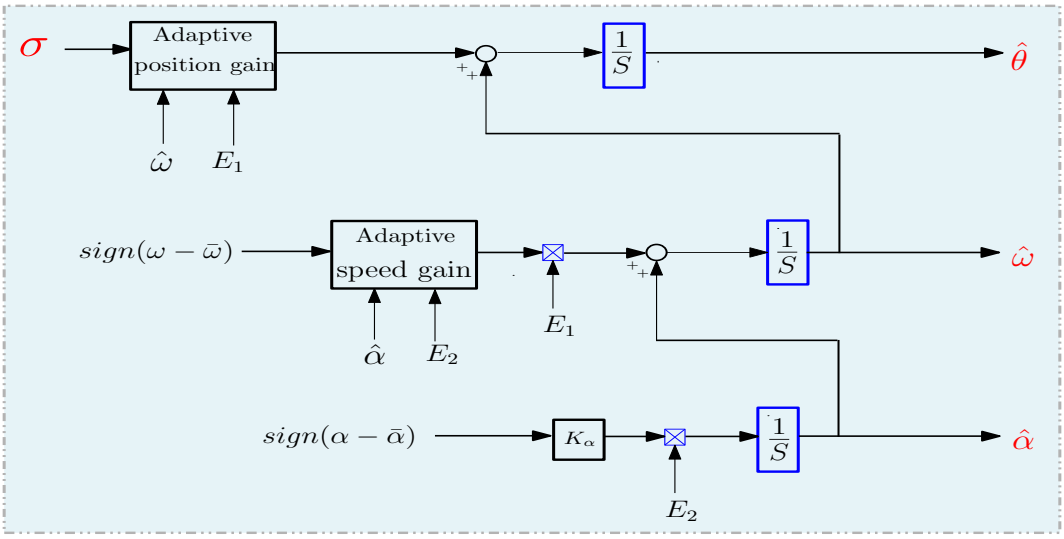

Figure 5: Block-diagram of adaptive step-by-step sliding mode tracking algorithm.

Theorem 1. *Consider system (43)–(45) where E_1 and E_2 (35,36) are defined according to the function $g(k)$ (37). Then, $\forall$ $K_{\theta_{max}} = 2\ \omega_{max} > max\{|e_\omega|\}$, $K_{\omega_{max}} = 2\ \alpha_{max} > max|\{e_\alpha|\}$, $K_\alpha > 0$, $K_{\theta_{min}} = \omega_{max} > max\{|\omega|\}$, $K_{\omega_{min}} = \alpha_{max} > max\{|\alpha|\}$, $K_{\theta_{min1}} > 0$ and $K_{\omega_{min1}} > 0$, system (43)–(45) converge to zero in finite-time, where $max\{|\omega|\}$, $max\{|e_\omega|\}$, $max\{|\alpha|\}$ and $max\{|e_\alpha|\}$ are the upper bounds of speed, acceleration, speed estimation error (41) and acceleration estimation error (42).*

proof: Let $K_{\theta_{max}}$, $K_{\omega_{max}}$, K_α, $K_{\theta_{min}}$, $K_{\omega_{min}}$, $K_{\theta_{min1}}$and $K_{\omega_{min1}}$ satisfying theorem conditions. Firstly, the stability of the position estimation error dynamic (43) is analyzed. Considering the nonempty manifold $S = \{e_\theta / e_\theta = 0\}$ and the following candidate Lyapunov function V_θ

$$V_\theta = \frac{1}{2} e_\theta^2. \tag{46}$$

One proves the attractivity of S as follows

$$\begin{aligned} \dot{V}_\theta &= e_\theta \dot{e}_\theta \\ &= e_\theta (e_\omega - [K_{\theta_{max}} - E_1\ f_1] sign(e_\theta)) \\ &= e_\theta e_\omega - e_\theta [K_{\theta_{max}} - E_1 f_1] sign(e_\theta) \\ &\leq |e_\theta||e_\omega| - [K_{\theta_{max}} - E_1\ f_1]|e_\theta|. \end{aligned} \tag{47}$$

Position transient ranges: As it can be seen on equation (37), in transient ranges $g(k) \neq 0$, then, $E_1 = 0$ the equation (47) can be written

$$\dot{V}_\theta \leq |e_\theta||e_\omega| - K_{\theta_{max}}|e_\theta|. \tag{48}$$

Let be $K_1 = -|e_\omega| + K_{\theta_{max}}$, as $K_{\theta_{max}} = 2\omega_{max} > max(|e_\omega|)$, $K_1 > 0$, then (48) can be written as

$$\dot{V}_\theta \leq -K_1|e_\theta|. \tag{49}$$

Position steady state ranges: In steady state, the sliding condition for (19) is achieved thus $E_1 = 1$, then

$$\dot{e}_\theta = e_\theta = 0. \tag{50}$$

By using (50) in (43), one can deduce

$$e_\omega = [K_{\theta_{max}} - f_1]sign(e_\theta). \tag{51}$$

Therefore, $\forall\ t \geq t_1$, the observer output $\bar{\omega}$ defined in (33) is equal to ω ($\bar{\omega} = \omega$), $sign(e_\theta) = sign(e_\omega)$ and $E_1 = 1$, for that, an adaptive rotor position gain estimation can be chosen to verify (52)

$$\dot{V}_\theta \leq |e_\theta||e_\omega| - [K_{\theta_{max}} - f_1]|e_\theta|. \tag{52}$$

By replacing f_1 defined in (29), (52) becomes

$$\dot{V}_\theta \leq |e_\theta||e_\omega| - [K_{\theta_{min}} + (K_{\theta_{min1}} - K_{\theta_{min}})\frac{|\hat{\omega}|}{\omega_{max}}]|e_\theta| \tag{53}$$

If $\hat{\omega} = 0$, by replacing this condition in (53), one can obtain

$$\dot{V}_\theta \leq |e_\theta||\omega| - K_{\theta_{min}}|e_\theta|. \tag{54}$$

Set $K'_1 = -|\omega| + K_{\theta_{min}}$. From theorem conditions $K_{\theta_{min}} > \omega_{max}$, $K'_1 > 0$, then one has

$$\dot{V}_\theta \leq -K'_1|e_\theta|. \tag{55}$$

If $\hat{\omega} = \omega_{max}$ and $|e_\omega| \approx 0$, by replacing this condition into (53), one can obtain

$$\dot{V}_\theta \leq -K_{\theta_{min1}}|e_\theta|. \tag{56}$$

From theorem conditions, the gain $K_{\theta_{min1}}$ is chosen to verify $K_{\theta_{min1}} > 0$ and sufficiently small to reduce the chattering effect. Inequalities (49), (55) and (56) prove the finite time convergence of the position estimation error e_θ to zero in transient/steady state position ranges for $t_1 > 0$. Figure 6 shows the adaptive gain K_θ with respect to the estimated speed. On this Figure it can be seen that, the position gain takes its maximum value $2\omega_{max}$ in transient modes. When the motor is operated in steady state ranges, the position gain varies between $K_{\theta_{min}}$ and ϵ_{θ_1} according to the estimated speed value.

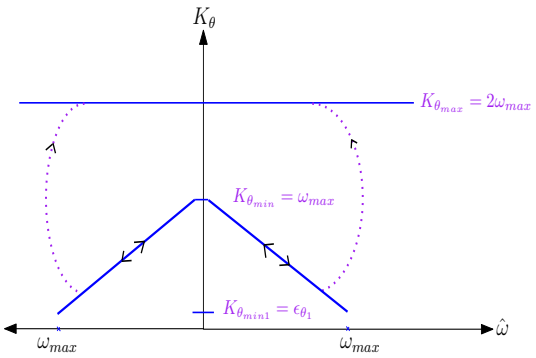

Figure 6: Adaptive position gain in different estimated speed ranges.

In the same manner, the stability of (44) can be proven.
In steady rotor position state, $\forall\ t \geq t_1$, the observer output $\bar{\omega}$ defined in (33) is equal to ω ($\bar{\omega} = \omega$), as one have $[K_{\theta_{max}} - E_1\ f_1] > 0$ and $E_1 = 1$, then

$$sign(e_\theta) = sign(e_\omega). \tag{57}$$

Therefore, the equation (57) is called the "sign propagation rule".
Consider the following candidate Lyapunov function

$$V_\omega = \frac{1}{2} e_\omega^2. \tag{58}$$

The time derivative of (58) is given as follows

$$\begin{aligned} \dot{V}_\omega &= e_\omega \dot{e}_\omega \\ &= e_\omega (e_\alpha - E_1 [K_{\omega_{max}} - E_2\ f_2] sign(\bar{\omega} - \hat{\omega})). \end{aligned} \tag{59}$$

With $\bar{\omega} = \omega$ and $E_1 = 1$, (59) reads

$$\begin{aligned} \dot{V}_\omega &= e_\omega e_\alpha - e_\omega [K_{\omega_{max}} - E_2\ f_2] sign(e_\omega) \\ &\leq |e_\omega||e_\alpha| - [K_{\omega_{max}} - E_2\ f_2]|e_\omega|. \end{aligned} \tag{60}$$

Speed transient ranges: In transient ranges, $E_2 = 0$, the equation (60) can be written

$$\dot{V}_\omega \leq |e_\omega||e_\alpha| - K_{\omega_{max}}|e_\omega|. \tag{61}$$

Let be $K_2 = -|e_\alpha| + K_{\omega_{max}}$. Then from theorem conditions $K_{\omega_{max}} > max(|e_\alpha|)$, $K_2 > 0$, and (61) becomes

$$\dot{V}_\omega \leq -K_2|e_\omega|. \tag{62}$$

Speed steady state ranges: In steady state, the sliding condition for (41) is achieved thus $E_2 = 1$, then,

$$\dot{e}_\omega = e_\omega = 0. \tag{63}$$

By replacing (63) in (44), one can deduce

$$e_\alpha = [K_{\omega_{max}} - \ f_2] sign(e_\omega). \tag{64}$$

Therefore, $\forall\ t \geq t_2$, the observer output $\bar{\alpha}$ defined in (34) is equal to α ($\bar{\alpha} = \alpha$), $sign(e_\omega) = sign(e_\alpha)$ and $E_2 = 1$. For that, an adaptive rotor speed gain estimation can be chosen to verify the following equation

$$\dot{V}_\omega \leq |e_\omega||e_\alpha| - [K_{\omega_{max}} - \ f_2]|e_\omega|. \tag{65}$$

By replacing f_2 defined in (31), (65) goes with

$$\dot{V}_\omega \leq |e_\omega||e_\alpha| - [K_{\omega_{min}} + (K_{\omega_{min1}} - K_{\omega_{min}})\frac{|\hat{\alpha}|}{\alpha_{max}}]|e_\omega|. \quad (66)$$

If $\hat{\alpha} = 0$, by replacing this condition in (66), one can obtain

$$\dot{V}_\omega \leq |e_\omega||\alpha| - K_{\omega_{min}}|e_\omega|. \quad (67)$$

Set $K'_2 = -\alpha_{max} + K_{\omega_{min}}$. Then, from theorem conditions $K_{\omega_{min}} > \alpha_{max}$, $K'_2 > 0$, one has

$$\dot{V}_\omega \leq -K'_2|e_\omega|. \quad (68)$$

If $\hat{\alpha} = \alpha_{max}$ and $|e_\alpha| \approx 0$, by replacing these conditions into (66), one can obtain

$$\dot{V}_\omega \leq -K_{\omega_{min1}}|e_\omega|. \quad (69)$$

From theorem conditions, the gain $K_{\omega_{min1}}$ is chosen to verify $K_{\omega_{min1}} > 0$ and sufficiently small to reduce the chattering effect. From inequalities (62), (68) and (69), the finite time convergence of the speed estimation error e_ω to zero is proved in transient/steady state ranges for $t_2 > t_1$. Figure 7 shows the adaptive gain K_ω with respect to the estimated acceleration. On this Figure, it can be seen that the speed gain takes its maximum value $2\alpha_{max}$ in transient modes. When the motor is operated in steady state ranges, the speed gain varies between $K_{\omega_{min}}$ and ϵ_{ω_1} according to the estimated acceleration value.

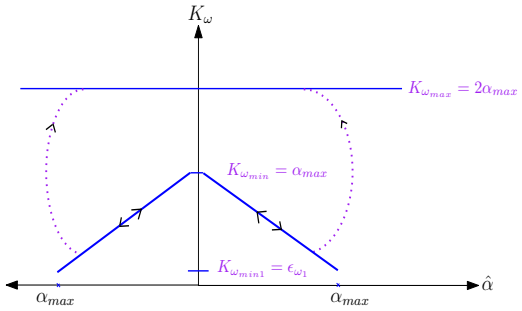

Figure 7: Adaptive speed gain in different estimated acceleration ranges.

In the same manner, the stability of (45) can be proven. Let V_α be the candidate Lyapunov function

$$V_\alpha = \frac{1}{2}e_\alpha^2. \quad (70)$$

The time derivative of (70) is

$$\begin{aligned} \dot{V}_\alpha &= e_\alpha \dot{e}_\alpha \\ &= e_\alpha(-E_2 K_\alpha sign(\bar{\alpha} - \hat{\alpha})). \end{aligned} \quad (71)$$

As $\bar{\alpha} = \alpha$ and $E_2 = 1$, (71) reads

$$\begin{aligned} \dot{V}_\alpha &= -e_\alpha K_\alpha sign(e_\alpha) \\ &\leq -K_\alpha|e_\alpha|. \end{aligned} \quad (72)$$

From theorem conditions $K_\alpha > 0$. This proves the finite time convergence of the acceleration estimation error e_α to zero in $t_3 > t_2$.
Inequalities (49), (55)-(56) (for position), (62), (68)-(69) (for speed) and (72) (for acceleration) prove the stability in finite-time of the proposed observer (28)–(32). □

Remark 2. *The proof of Theorem 1 is obtained by considering that the ideal sliding motion (invariance) is reached [39] with respect to the estimation error. However, in practice as the error oscillates around zero, the ideal sliding motion can be reached by considering the average value of the estimation error.*

5.3. Parameters Tuning

- Parameters $K_{\theta_{max}}$, $K_{\omega_{max}}$, K_α, $K_{\theta_{min}}$,$K_{\omega_{min}}$, $K_{\theta_{min1}}$ and $K_{\omega_{min1}}$ are chosen according to the stability analysis given in section *2.2.2* in order to ensure the finite time convergence of the observer in both transient/steady state modes.

- Parameters ϵ_{θ_1},ϵ_{ω_1} and ϵ_α are chosen sufficiently small to reduce the chattering phenomenon, because their effects appear only in steady-state operating modes.

- The characteristics of the HF injected voltage, defined in (22), verify the following properties. The frequency ($w_c = 2\,\pi\,f_c$) should be less than the half of the inverter one and higher than the machine nominal one. The injected magnitude (V_c) should be chosen as low as possible to minimize torque ripples and to reduce the machine warming.

6. Simulation and Experimental Results

Performances of the developed self-sensing control strategy are evaluated through simulation and experimental tests and a comparison study with algorithms introduced in subsection 2 is conducted.

6.1. Test Bench (http://www2.irccyn.ec-nantes.fr/BancEssai/)

The test bench is made up of a rated 3 kW target Interior Permanent Magnet Synchronous Motor (IPMSM), a type of AC salient pole machines, with an incremental coder as position sensor which is used only for the comparison purpose. A dSPACE board DSP1103 is used to carry out the real time algorithm. The converter is composed of a three-phase IGBT power module from (SEMIKRON), a DC-link voltage sensor and protection circuits. IPMSM parameters are shown in Table 1 and the control parameters are shown in Table 2.

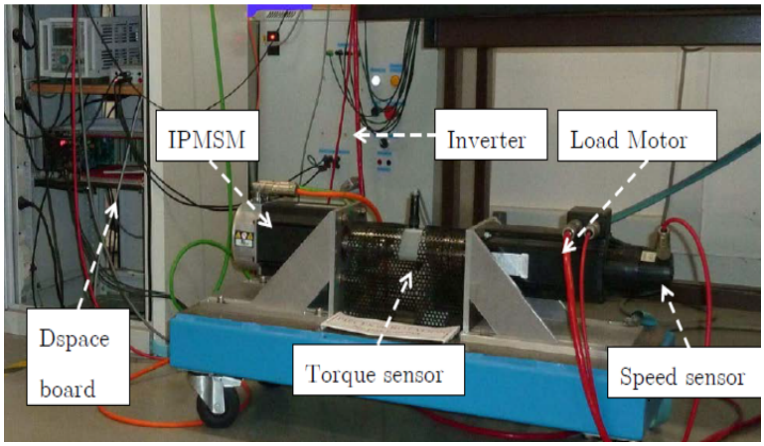

Figure 8: Experimental test bench

In order to evaluate the performance and the effectiveness of the proposed strategy in realistic situation, a representative cycle of drive benchmark shown in Figure 9 is considered and the applied torque is shown. These profiles are defined by industrials for automotive applications. The objective is to test the motor in different possible speed/torque ranges. At the beginning, the IPMSM is operated at zero speed and maximum torque which represents a difficult test in automotive applications. From 3.2 s to 4 s, the developed self-sensing strategy is evaluated at nominal speed with nominal torque. Then, the motor is operated at zero speed without torque from 4.9 s to 5.5 s which allows to evaluate the performance of the developed strategy in critical observability areas. The gain I_{cn} defined in (21) is a function of the machine inductances, which can vary significantly depending on the operation conditions (temperature variations, magnetic circuit saturation,...) and on injected signal characteristics. As pointed out earlier, the developed self-sensing strategy is independent from machine parameters (mainly inductances and mechanical time-constant mismatches). To highlight this independence, an arbitrary I_{cn} profile (Figure 10) and an arbitrary mechanical time-constant (Figure 11) are defined.
For simulation tests (to be closer to the realistic situation) a white noise is added to current measurements.

Table 1: Motor parameters

Speed	2100 RPM	Torque	$9Nm$
J	7.3 10^{-3} $kg.m^2$	Φ_f	0.33 Wb
R_s	1.4 Ω	L_d	5.7 mH
p	3	L_q	9.9 mH

Table 2: Parameters of the control system

Inverter switching Frequency	10 kHz	Injected voltage frequency	$V_c = 2\ V$, $f_c = 1$ kHz
DC bus voltage	400 V	$K_{\theta_{max}}$, $K_{\omega_{max}}$, K_α	250, 110, 90
PLL gains $(K_{\omega,p}, K_{\theta,P})$	40, 650	Sampling period	10^{-4} s
MSO gains $(K_{\theta,s}, K_{\omega,s}, K_{T,s})$	30, 275, 3	$K_{\theta_{min}}$,$K_{\omega_{min}}$	110, 280
$K_{\theta_{min1}}$ and $K_{\omega_{min1}}$	5	Noise magnitude	0.8 A

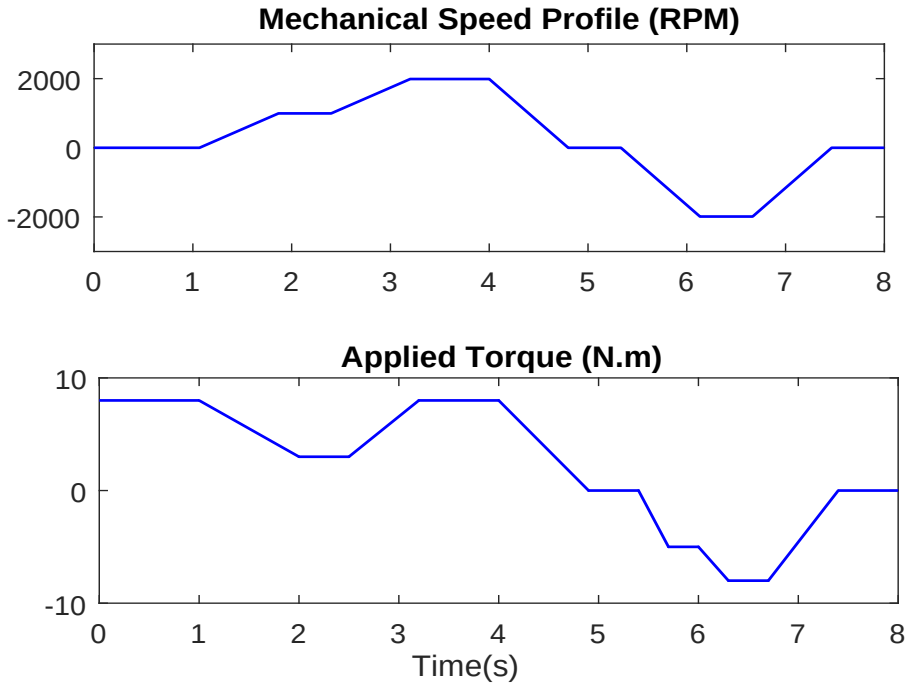

Figure 9: Drive benchmark cycle

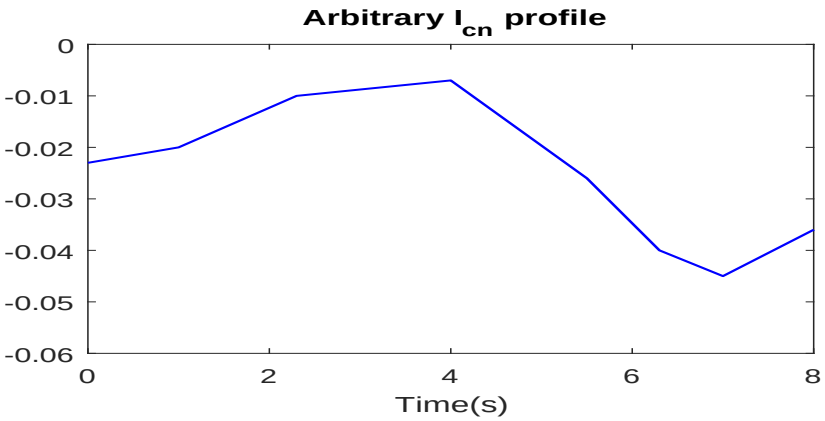

Figure 10: Arbitrary I_{cn} profile

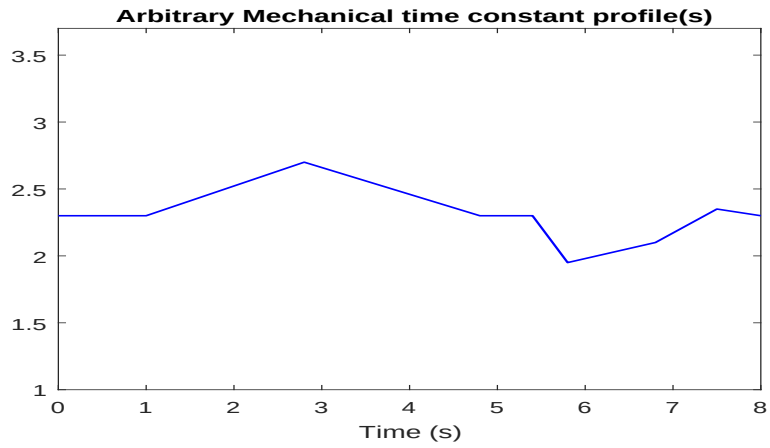

Figure 11: Arbitrary mechanical time constant

6.2. Results of the proposed estimation strategy

Simulation (Figure 13) and experimental (Figure 12) results of the motivating idea proposed in this paper show the evolution of these quantities: the measured and the estimated mechanical speeds, the mechanical speed estimation error, the measured and the estimated electrical positions, the electrical position estimation error and the estimated acceleration of the machine.
In simulation step, the inductances variation on I_{cn} (Figure 10) and variations on the mechanical constant time (inertia and viscous coefficient) (Figure 11) are considered.
It can be seen, from simulation and experimental results (Figure 13 and Figure 12), that

- Convenient rotor position and speed estimation results are obtained in all speed/torque ranges even in difficult situations mentioned on the cycle of drive benchmark (Figure 9).
- The acceleration is well estimated, this enables to get an enhanced rotor position and speed estimation even in acceleration modes (transients modes).

- The electrical position estimation error is centered around zero with the highest noise peak does not exceed a threshold of 2 degrees for simulation results and 4 degrees for experimental results.
- The mechanical speed estimation error is centered around zero with highest noise peak that does not exceed a threshold of $4RPM$ for simulation results and $8RPM$ for experimental ones.
- the chattering effect is reduced in comparison to the results of the step-by-step observer with constant gains (see Figures 12 and 16).
- The proposed observer gives good estimations in critical observability area (from 4.9s to 5.5s) because in this area as it is proved in [40], the AC motors are observables when the HF injected signal is used.

As a conclusion, very acceptable results are obtained in simulation (Figure 13) and experimental (Figure 12) tests at different speed/torque ranges despite the variations of inductances and mechanical constant time, which confirms the machine parameters insensitivity of the procedure estimation strategy enhanced in subsection 5.1 (Part 1).
However, small noisy position and speed errors can be seen in simulation and experiments. These errors are more affected in experiments compared to simulation. The reason is that in simulation only the effect of the chattering is acting, which is well reduced by the proposed adaptive observer of subsection 5.2 (Part 2), while in experiments other parameters are acting such that the HF injected signal that generates harmonics and the inverter effect.

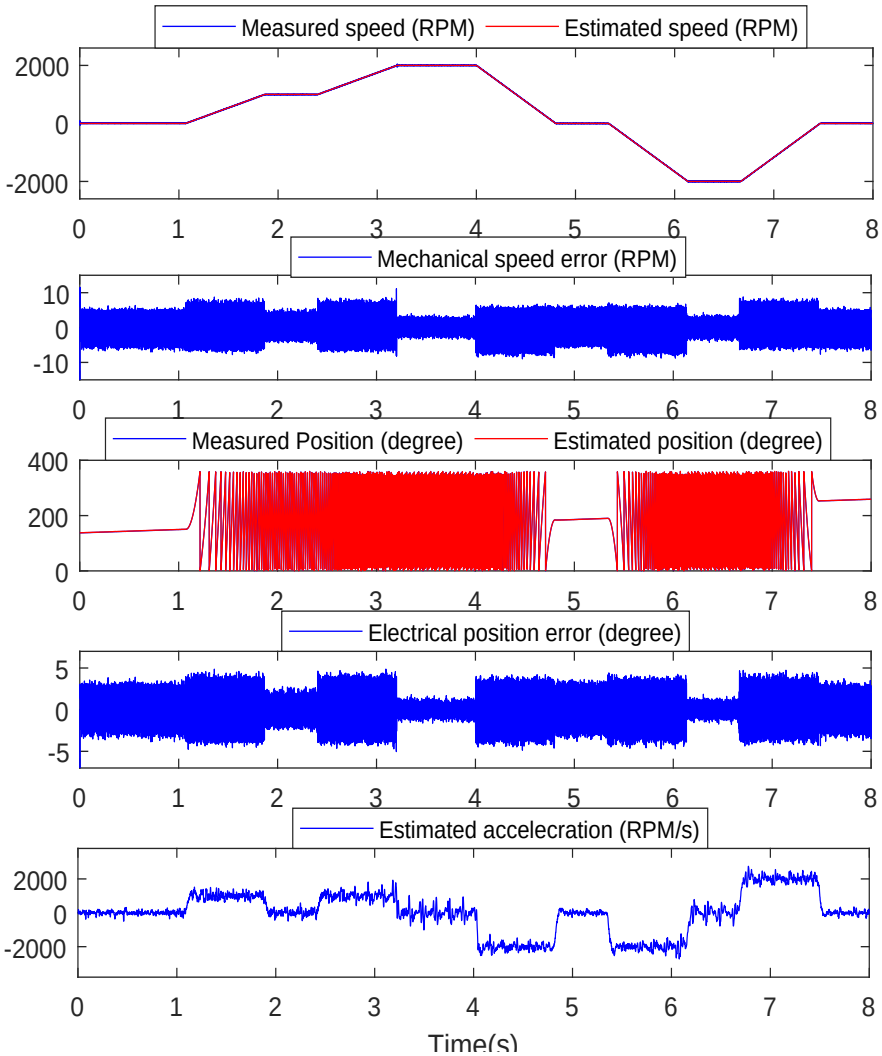

Figure 12: Experimental results of the proposed algorithm.

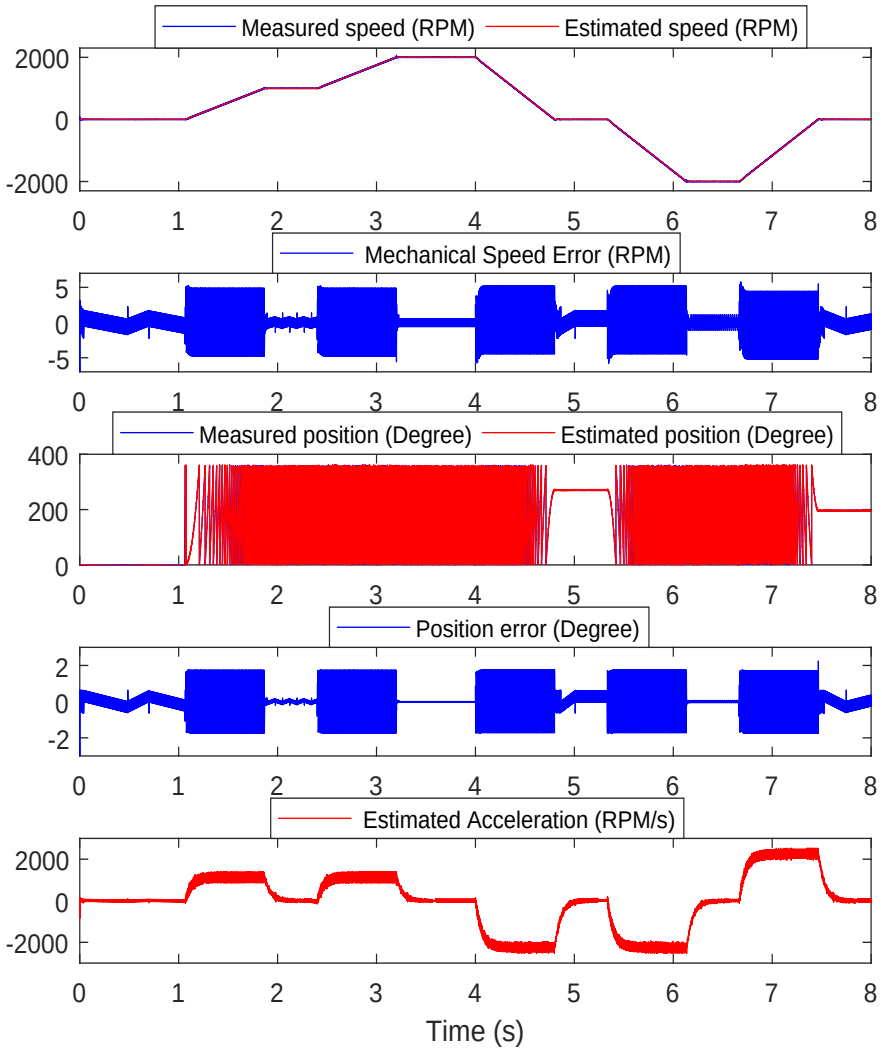

Figure 13: Simulation results of the proposed algorithm.

6.3. Comparative study

Several simulations have been made in order to compare the proposed self-sensing strategy with the classical tracking algorithms, PLL ((1)-(2)) and MSO ((3)-(4)), recalled in section 2 and the step-by-step observer with constant gains given in [24].

6.3.1. Comparison with PLL and MSO strategies

For the first evaluation, the PLL algorithm is tested with nominal machine parameters (without considering the I_{cn} profile in Figure 10). From the obtained results (Figure 15), one can observe an important rotor position and speed estimation errors during transients. It confirms its sensitivity to acceleration effect. After that, a simulation was conducted by considering the I_{cn} profile in Figure 10 (inductance variations). In this case, the estimated rotor position and speed diverge immediately. It highlights the sensitivity of the PLL algorithm with respect to the parameter (inductances) variations. As mentioned in section 2,

the MSO depends on the mechanical machine parameters (inertia and viscous coefficient), which can vary significantly according to several unpredictable effects such as the applied load torque, weight, road type and tires quality in automotive applications. That is why a comparison study is made between the proposed strategy and the MSO with respect to the mechanical parameters. The relationship between the speed and the torque balance can be represented by the following transfer function

$$\frac{\hat{\omega}(s)}{T_m - \hat{T}_l} = \frac{K_{stat}}{s\tau + 1}$$

where $K_{stat} = \frac{1}{K_f}$ and $\tau = \frac{J}{K_f}$ are the static gain and the time constant of this transfer,respectively. In addition, gains of the MSO are computed according to the inertia and friction coefficient that makes its tuning more difficult and could cause a stability problem. For this study, an arbitrary profile, shown in Figure 11 of the mechanical time constant is considered in simulation. Results of this simulation presented in Figure 14 show that the MSO can give good rotor and speed estimation when the nominal mechanical time constant is used ($t \in [0,\ 1] \cup [4.9,\ 5.5] \cup [7.6,\ 8]$). Important estimation errors can be noticed on the rotor position and speed obtained by the MSO when the considered mechanical time constant is biased.
Note that this test is obtained without considering I_{cn} profile, once this latter is considered, the estimated rotor position and speed diverge immediately.
The robustness comparative study between the proposed algorithm and the classical tracking algorithms is summarized in Table 3.

Table 3: Summary of the comparative study

Robustness vs	Proposed Algorithm	MSO	PLL
Mechanical parameters	Independent	Dependent	Independent
Electrical parameters	Independent	Dependent	Dependent
Maximal rotor position estimation error (Degree)	4	25	30
Maximal speed estimation error (RPM)	7	45	50
Machine acceleration	Insensitive	Sensitive	Very sensitive

This comparative study confirms that the developed self-sensing strategy offers a significant and attractive improvement compared to the previous methods.

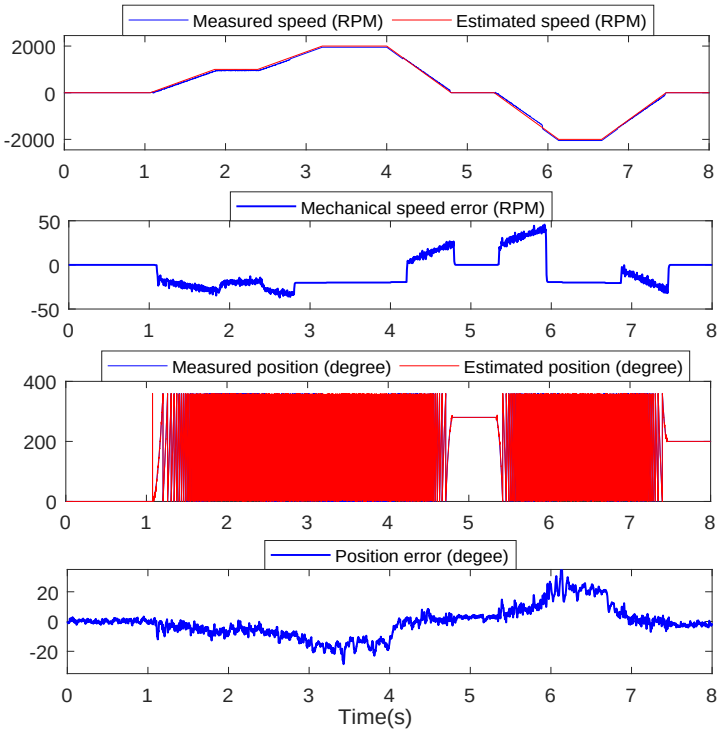

Figure 14: MSO simulation results with mechanical time constant variation defined in Figure (11).

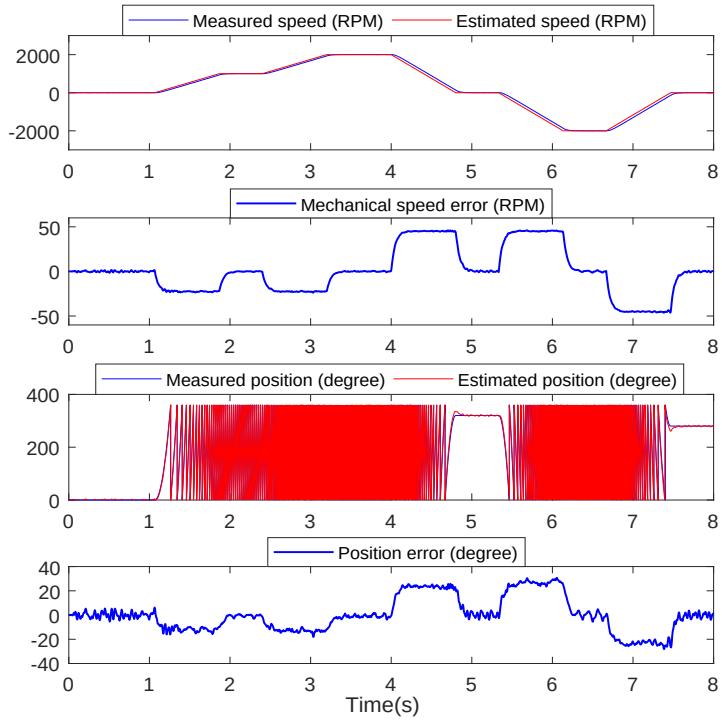

Figure 15: PLL simulation results (without considering the I_{cn} variations)

6.3.2. Comparison with constant gains step-by-step sliding mode observer

The constant gains step-by-step observer is tested experimentally in order to test its performances with respect to the proposed observer

It can be seen that the step-by-step sliding mode observer with constant gains (Figures 16) is sensitive to chattering generated by important imposed gains, the estimated rotor position is noisy that can affect the control algorithm. However, the proposed adaptive gains step-by-step observer reduces (Figures 12 and 13) the chattering effects on the rotor position and speed estimation.

This comparative study between the proposed adaptive step-by-step sliding mode observer ((28)–(32)) and the step-by-step one with constant gains [24] in terms of machine parameters sensitivity, chattering, and estimation error accuracy is summarized in the Table 4.

Table 4: Summarize of the comparative study between adaptive and constant gains step-by-step observers

Robustness vs	Adaptive step-by-step observer	step-by-step observer
Electrical parameters	Independent	Independent
Mechanical parameters	Independent	Independent
Chattering effect	Insensitive	Sensitive
Maximal rotor position estimation error (Degree)	4	15
Maximal speed estimation error (RPM)	7	20
Machine acceleration	Insensitive	Insensitive

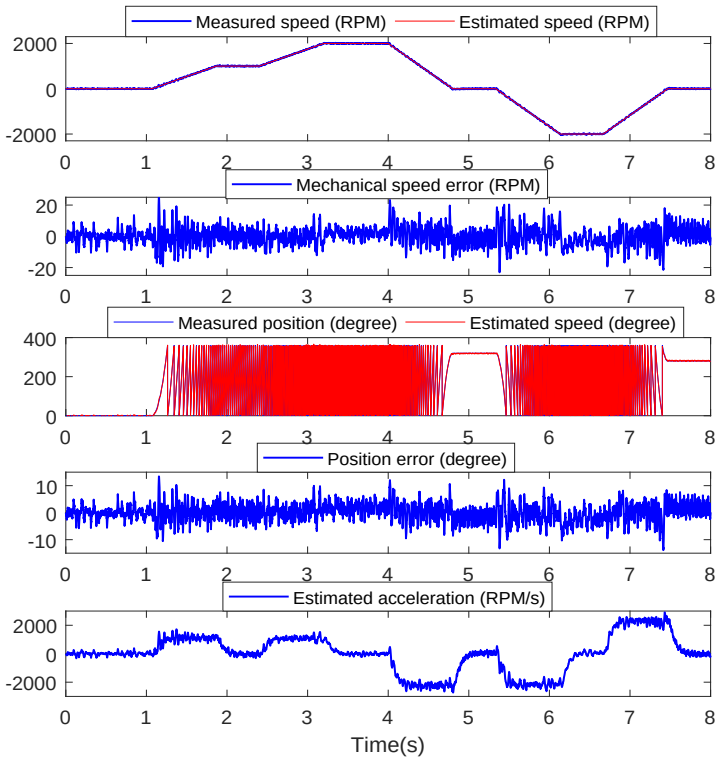

Figure 16: Experimental result of the step-by-step sliding mode observer with constant gains.

7. Conclusion

This paper presented a novel approach for tracking algorithms associated to HF signal injection methods in order to estimate the rotor position of sensorless AC salient pole machines. The main benefit of this approach is to use only the sign of the rotor position estimation error as a known information instead of the rotor position estimation error used by the classical tracking algorithms. By doing so, both advantages of parameters insensitivity and removing the LPFs used to extract the rotor position estimation error are achieved. As only the sign of the error position is available, the first order sliding mode observer is the natural choice to estimate the rotor position. However, in this paper an adaptive step-by-step sliding mode observer is proposed as an alternative solution to reduce the chattering phenomena. The stability of the proposed observer is proven in transient and steady state ranges. The performances of the proposed approach are highlighted in simulation and in experiments performed at a representative small-scale electric propulsion used in automotive applications. The comparative study with respect to the principal existing tracking algorithms illustrates the effectiveness of the proposed methodology.

Acknowledgement

This work was supported by the Chair between Renault and Centrale Nantes for the improvement of EV/HEV propulsion performances.

References

[1] E. Trancho, E. Ibarra, A. Arias, I. Kortabarria, P. Prieto, I. M. de AlegrÃa, J. Andreu, I. López, Sensorless control strategy for light-duty evs and efficiency loss evaluation of high frequency injection under standardized urban driving cycles, Applied Energy 224 (2018) 647 – 658.

[2] Z. Chen, L. Wang, X. Liu, Sensorless direct torque control of pmsm using unsected kalman filter*, IFAC Proceedings Volumes 44 (1) (2011) 4380 – 4385, 18th IFAC World Congress.

[3] M.-G. Gan, M. Zhang, C.-Y. Zheng, J. Chen, An adaptive sliding mode observer over wide speed range for sensorless control of a brushless dc motor, Control Engineering Practice 77 (2018) 52 – 62.

[4] M. A. Hamida, J. De Leon, A. Glumineau, R. Boisliveau, An adaptive interconnected observer for sensorless control of pm synchronous motors with online parameter identification, IEEE Transactions on Industrial Electronics 60 (2) (2013) 739–748.

[5] M. Hamida, J. de Leon, A. Glumineau, Experimental sensorless control for ipmsm by using integral backstepping strategy and adaptive high gain observer, Control Engineering Practice 59 (2017) 64 – 76.

[6] A. Messali, M. A. Hamida, M. Ghanes, M. Koteich, A novel high frequency signal injection strategy for self-sensing control of electric ac machine drives, in: IECON 2018 - 44th Annual Conference of the IEEE Industrial Electronics Society, 2018, pp. 343–348.

[7] J. Chen, J. Huang, Y. Sun, Resistances and speed estimation in sensorless induction motor drives using a model with known regressors, IEEE Transactions on Industrial Electronics 66 (4) (2019) 2659–2667.

[8] A. K. Jebai, F. Malrait, P. Martin, P. Rouchon, Signal injection and averaging for position estimation of Permanent-Magnet Synchronous Motors.

[9] G. Wang, L. Yang, G. Zhang, X. Zhang, D. Xu, Comparative investigation of pseudorandom high-frequency signal injection schemes for sensorless ipmsm drives, IEEE Transactions on Power Electronics 32 (3) (2017) 2123–2132.

[10] C. MartÃn, M. BermÃºdez, F. Barrero, M. R. Arahal, X. Kestelyn, M. J. DurÃ¡n, Sensitivity of predictive controllers to parameter variation in five-phase induction motor drives, Control Engineering Practice 68 (2017) 23 – 31.

[11] Y. Wang, Y. Xu, J. Zou, Sliding mode sensorless control of pmsm with inverter nonlinearity compensation, IEEE Transactions on Power Electronics (2019) 1–1.

[12] M. Abdelrahem, A. E. Hafni, R. Kennel, C. M. Hackl, Predictive phase locked loop for sensorless control of pmsg based variable-speed wind turbines, in: 2017 IEEE International Symposium on Sensorless Control for Electrical Drives (SLED), 2017, pp. 151–156.

[13] M. Abdelrahem, C. M. Hackl, R. Kennel, Finite position set-phase locked loop for sensorless control of direct-driven permanent-magnet synchronous generators, IEEE Transactions on Power Electronics 33 (4) (2018) 3097–3105.

[14] K. B. Lee, J. Y. Yoo, J. H. Song, I. Choy, Improvement of low speed operation of electric machine with an inertia identification using roelo, IEE Proceedings - Electric Power Applications 151 (1) (2004) 116–120.

[15] P. L. Xu, Z. Q. Zhu, Novel square-wave signal injection method using zero-sequence voltage for sensorless control of pmsm drives, IEEE Transactions on Industrial Electronics 63 (12) (2016) 7444–7454.

[16] G. Zhen, W. Jianmin, Z. Xiaomin, Improved square-wave voltage injection method for sensorless control of pmsm and its adaptability to motor parameter variations, in: 2014 17th International Conference on Electrical Machines and Systems (ICEMS), 2014, pp. 710–715.

[17] Y. Yoon, S. Sul, S. Morimoto, K. Ide, High-bandwidth sensorless algorithm for ac machines based on square-wave-type voltage injection, IEEE Transactions on Industry Applications 47 (3) (2011) 1361–1370.

[18] V. Acary, B. Brogliato, Y. V. Orlov, Chattering-free digital sliding-mode control with state observer and disturbance rejection, IEEE Transactions on Automatic Control 57 (5) (2012) 1087–1101.

[19] M. T. Angulo, J. A. Moreno, L. Fridman, The differentiation error of noisy signals using the generalized super-twisting differentiator, in: 51st IEEE Conference on Decision and Control (CDC), IEEE, 2012.
[20] W. Perruquetti, J.-P. Barbot, Sliding mode control in engineering, CRC Press, 2002.
[21] I. Boiko, M. I. Castellanos, L. Fridman, Super twisting algorithm-based step-by-step sliding mode observers for nonlinear systems with unknown inputs., International Journal of Systems Science 38 (2007) 803–815.
[22] G. Bartolini, A. Ferrara, E. Usani, Chattering avoidance by second-order sliding mode control, Automatic control, IEEE Transactions on 43.
[23] C. Edwards, Y. B. Shtessel, Adaptive continuous higher order sliding mode control, Automatica 65 (2016) 183–190.
[24] T. Floquet, J.-P. Barbot, Super twisting algorithm based step-by-step sliding mode observers for nonlinear systems with unknown inputs, International Journal of Systems Science 38 (10) (2007) 803–815.
[25] L. Fridman, J. Moreno, R. Iriarte, Sliding Modes after the first Decade of the 21st. Century, Lecture Notes in Control and Information Sciences, Vol. 412, 2011.
[26] A. Levant, Chattering analysis, IEEE transactions on automatic control 55 (6) (2010) 1380–1389.
[27] F. Plestan, C. Evangelista, P. F. Puleston, I. Guenoune, Control of a twin wind turbines system without wind velocity information, in: 15th International Workshop on Variable Structure Systems, VSS 2018, Graz, Austria, July 9-11, 2018, 2018, pp. 150–155.
[28] M. Hamida, J. D. Leon, A. Glumineau, High-order sliding mode observers and integral backstepping sensorless control of ipms motor, International Journal of Control 87 (10) (2014) 2176–2193.
[29] A. Polyakov, D. Efimov, W. Perruquetti, Sliding mode control design for mimo systems: Implicit lyapunov function approach, 2014, pp. 2612–2617. doi:10.1109/ECC.2014.6862362.
[30] V. Utkin, Chattering problem, IFAC Proceedings Volumes 44 (1) (2011) 13374–13379.
[31] X.-G. Yan, S. K. Spurgeon, C. Edwards, Dynamic sliding mode control for a class of systems with mismatched uncertainty, European Journal of Control 11 (1) (2005) 1–10.
[32] O. Wallmark, L. Harnefors, O. Carlson, An improved speed and position estimator for salient permanent-magnet synchronous motors, IEEE Transactions on Industrial Electronics 52 (1) (2005) 255–262.
[33] R. D. Lorenz, K. V. Patten, High resolution velocity estimation for all digital, ac servo drives, in: Conference Record of the 1988 IEEE Industry Applications Society Annual Meeting, 1988, pp. 363–368 vol.1.
[34] G. Wang, L. Yang, G. Zhang, X. Zhang, D. Xu, Comparative investigation of pseudorandom high-frequency signal injection schemes for sensorless ipmsm drives, IEEE Transactions on Power Electronics 32 (3) (2017) 2123–2132.
[35] T. H. Liu, S. K. Tseng, T. W. Lin, J. L. Chen, Sensorless ipmsm position control system using a high frequency injection method, in: 2016 IEEE 2nd Annual Southern Power Electronics Conference (SPEC), 2016, pp. 1–6.
[36] J.-I. Ha, S.-K. Sul, Sensorless field-orientation control of an induction machine by high-frequency signal injection, IEEE Transactions on Industry Applications 35 (1) (1999) 45–51.
[37] M. J. Corley, R. D. Lorenz, Rotor position and velocity estimation for a salient-pole permanent magnet synchronous machine at standstill and high speeds, IEEE Transactions on Industry Applications 34 (4) (1998) 784–789.
[38] A. F. Filippov, Differential Equations with Discontinuous Right-Hand Side, Vol. 2, 1960. doi:10.1007/978-94-015-7793-9.
[39] G. Bartolini, L. Fridman, A. Pisano, E. Usai, Modern Sliding Mode Control Theory. New Perspectives and Applications, Vol. 375, 2008. doi:10.1007/978-3-540-79016-7.
[40] M. Koteich, A. Maloum, G. Duc, G. Sandou, Observability analysis of sensorless synchronous machine drives, in: 2015 European Control Conference (ECC), 2015, pp. 3560–3565.